

EA-BEV: Edge-aware Bird’s-Eye-View Projector for 3D Object Detection

Haotian Hu

hht1996ok@zju.edu.cn

Fanyi Wang

11730038@zju.edu.cn

Jingwen Su

j_su95@outlook.com

Laifeng Hu

hlf@alu.uestc.edu.cn

Tianpeng Feng

tianpeng_feng@whu.edu.cn

Zhaokai Zhang

zhangzhaokai1@oppo.com

Wangzhi Zhang*

zhiwang.zhang@sydney.edu.au

Abstract

In recent years, great progress has been made in the Lift-Splat-Shot-based (LSS-based) 3D object detection method, which converts features of 2D camera view and 3D lidar view to Bird’s-Eye-View (BEV) for feature fusion. However, inaccurate depth estimation (e.g. the “depth jump” problem) is an obstacle to develop LSS-based methods. To alleviate the “depth jump” problem, we proposed Edge-Aware Bird’s-Eye-View (EA-BEV) projector. By coupling proposed edge-aware depth fusion module and depth estimate module, the proposed EA-BEV projector solves the problem and enforces refined supervision on depth. Besides, we propose sparse depth supervision and gradient edge depth supervision, for constraining learning on global depth and local marginal depth information. Our EA-BEV projector is a plug-and-play module for any LSS-based 3D object detection models, and effectively improves the baseline performance. We demonstrate the effectiveness on the nuScenes benchmark. On the nuScenes 3D object detection validation dataset, our proposed EA-BEV projector can boost several state-of-the-art LSS-based baselines on nuScenes 3D object detection benchmark and nuScenes BEV map segmentation benchmark with negligible increment of inference time. Code to reproduce our results is available at <https://github.com/hht1996ok/EA-BEV>.

1. Introduction

With the increasing complexity of autonomous driving and vehicle sensors, it is crucial to integrate multiple sources of information (e.g. the 2D multi-view images from the camera and point clouds from lidar) from different sensors and derive a unified representation of features. It is a trend to project different sources of information to Bird’s-

Eye-View (BEV), and attracts a great deal of attention from both academia and industry. One of the core challenges of BEV perception is how to reconstruct the lost depth information of 2D images, and provide accurate feature distribution for subsequent networks.

Lift-Splat-Shot-based (LSS-based) methods [8, 7, 31, 25] predict depth distribution of each grid on 2D features, and “lifts” the 2D features of each grid into the voxel space by using predicted depth distribution. However, due to the large depth difference between some regions of 2D images, it is difficult for depth estimation module to accurately learn depth distribution, resulting in shift or loss of object edge semantic information in the voxel. And we refer to this problem as “depth jump”. As shown in Figure 1 (b), the black vacant area of foreground vehicle edges in red box indicates that the depth estimation module of previous LSS-base method (e.g., BEVFusion [31]) has a poor performance of fitting in the “depth jump” area. While after adding EA-BEV, fitting effect is significantly improved.

In addition, previous LSS-based methods can not fully utilize the depth information to supervise the depth estimation tasks. For example, BEVDet [7] does not take the depth information of the point cloud in consideration to constrain the depth estimation module. BEVFusion [31] uses the depth map projected from point clouds to implicitly supervise the depth estimation network, but without fully utilizing the accurate depth information. BEVDepth [25] employs min pooling and one-hot operations to align the predicted depth map with the projected depth map from the point clouds. However, the projected depth maps are extremely sparse after projected into 2D, which prevents the network from learning the correct depth estimations.

To alleviate the “depth jump” problem and better utilize the depth information to supervise depth prediction tasks, we proposed Edge-Aware Bird’s-Eye-View (EA-BEV) projector. As shown in Figure 1 (c), after using our proposed

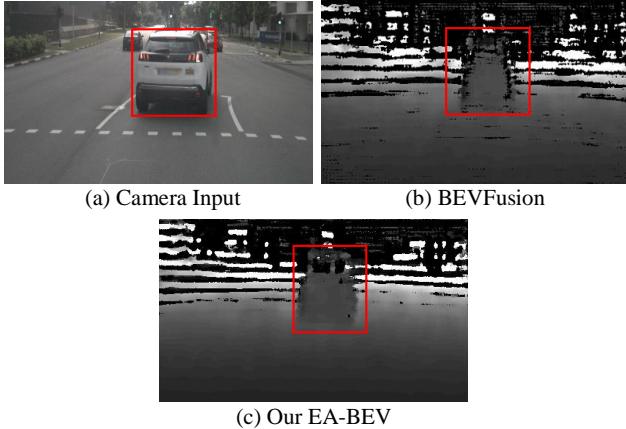


Figure 1. Visualisation of “depth jump” problem. It shows depth estimation before and after adding EA-BEV on baseline method BEVFusion [31]. The larger the pixel value, the deeper the depth.

EA-BEV projector, we have more accurate depth estimation on the foreground vehicle edges in red box. Our proposed EA-BEV projector is plug-and-play and can be used in any LSS-based methods. Moreover, we propose a edge-aware depth fusion module to alleviate the “depth jump” problem. By using additional geometry information of object edge (i.e. prior knowledge), our proposed edge-aware depth fusion module captures fine-grained local edge depth information. We also propose gradient edge depth supervision to better fit with rapid depth changes between objects. To fully utilize depth information for supervising depth prediction tasks, we propose a depth estimation module by adding an 8x upsampling operation for sparse depth supervision.

In order to validate effectiveness and efficiency of our proposed EA-BEV projector, experiments are conducted on nuScenes dataset [4]. The proposed EA-BEV projector significantly improves performance of several state-of-the-art LLS-based baselines [7, 31, 25] while the increased inference time is negligible, which achieves the state-of-the-art performance on nuScenes 3D object detection validation set. Besides, to evaluate generalization capability of our proposed EA-BEV projector, we conduct experiments on nuScenes BEV map segmentation benchmarks.

The contributions of this paper are as follows:

1) To alleviate the “depth jump” problem and better utilize depth information for supervising the depth prediction tasks, we propose Edge-Aware Bird’s-Eye-View (EA-BEV) projector for 3D Object Detection task.

2) We propose edge-aware depth fusion module and gradient edge depth supervision to alleviate the “depth jump” problem, and depth estimation module to generate estimated depth distribution more accurately.

3) Extensive experiments demonstrate that our proposed EA-BEV projector can boost several state-of-the-art BEV

baselines on nuScenes 3D object detection benchmark and nuScenes BEV map segmentation benchmark with negligible increment of inference time.

2. Related Work

3D object detection is one of the core tasks of 3D perception, predicting object types and 3D bounding boxes. Previous works [23, 20] directly predict from perspective view (PV) features, which are unable to exploit stereo visual cues from multiple views and time-continuous frames. BEV-based 3D object detection models [31, 10, 2, 7] are beneficial to fuse multi-source and multi-timestamp features, and these models have made great progress in terms of efficiency and performance.

One of the core problems of BEV perception lies in reconstructing the lost 3D information using PV-to-BEV view translation. To compensate the difference between these two views, previous methods can be divided into network-based view transformation methods [12, 1, 32, 26, 24] and depth-based view transformation methods [7, 2, 28, 15, 21]. They are represented in Section 2.1 and Section 2.2, respectively.

2.1. Network-based View Transformation Methods

2.1.1 MLP-based Approach

MLP-based approaches use MLP to learn an implicit representation of camera calibration for conversion between two different views. HDMapNet [12] considers that one-way projection is difficult to ensure effective transfer during forward pass of view information from PV to BEV. Therefore, it also uses MLP to backward project features from BEV to PV. VED [1] is the first method using end-to-end learning on monocular images to generate semantic-metric occupancy grid map in real time. It converts PV feature maps into BEV feature maps through flattening, mapping, and reshaping operations for multi-modal perception and prediction.

2.1.2 Transformer-based Approach

Transformer-based approaches directly employs the transformer to map PV into BEV, which does not explicitly require the camera model. Tesla first uses the transformer to project PV features into the BEV. It adopts positional encoding to design a set of BEV queries, then performs view transformations through cross-attention mechanism between BEV queries and image features. BEVFormer [32] employs deformable attention to extract dense queries in the BEV and describes relationships between multi-view features. DETR3D [26] utilizes a geometry-based feature sampling process instead of cross-attention to predict 3D reference points, and projects reference points into the 2D

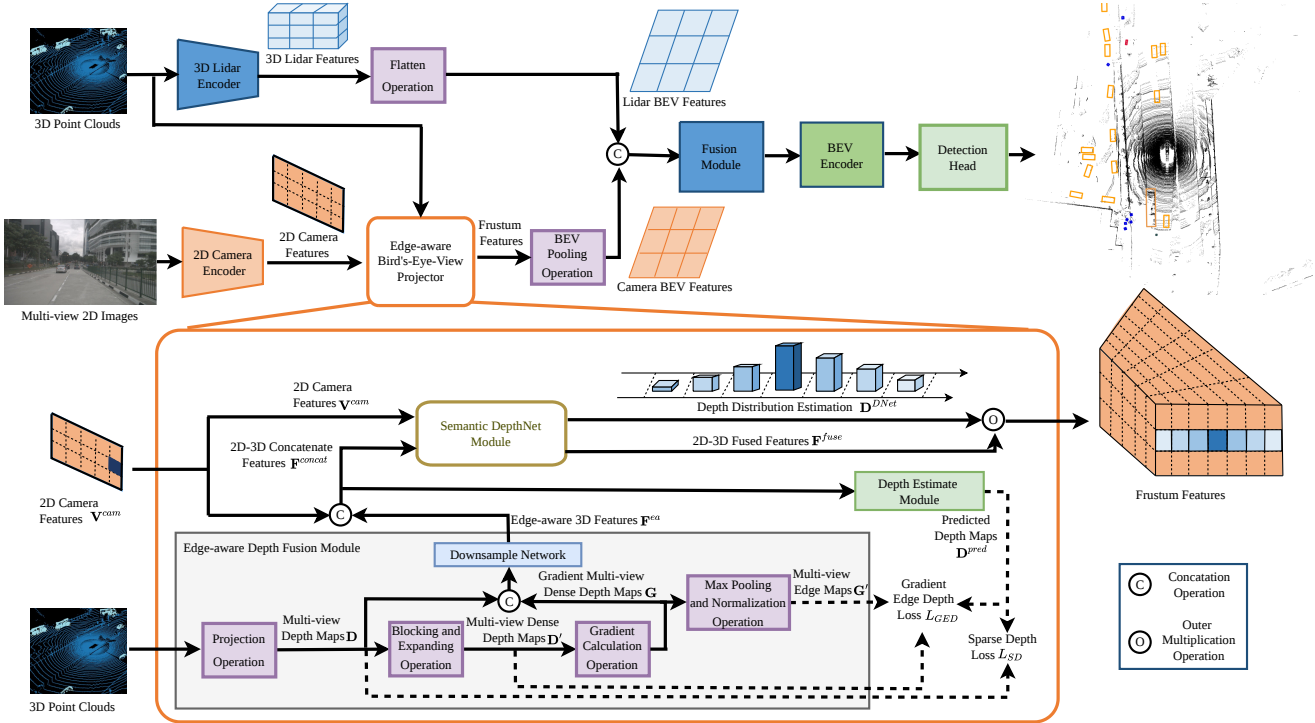


Figure 2. Overview of LSS framework [8] and our proposed EA-BEV projector. LSS framework uses both 2D input (i.e., 2D multi-view images from camera) and 3D input (i.e., point cloud from lidar) to generate bounding boxes of vehicle, pedestrian, etc. Our proposed EA-BEV projector (orange block) contains the proposed Edge-aware Depth Fusion Module (grey block), Semantic DepthNet Module (yellow block), and Depth Estimation Module (green block). Besides, the Sparse Depth Supervision and Gradient Edge Depth Supervision are represented with dotted arrows.

image plane using a calibration matrix to achieve end-to-end 3D edge prediction. PETrv2 [24] extends 3D position embedding to the time domain, effectively utilizing continuous frame information. PolarDETR [14] brings parameters of 3D object detection to the polar coordinate system, reformulating edge parameterization, network prediction and loss calculation.

2.2. Depth-based View Transformation

2.2.1 Point-based Approach

Point-based approaches use depth estimation to convert image pixels into pseudo-laser point clouds, and feed to a lidar-based 3D detector. However, these approaches are highly dependent on the accuracy of depth estimation. Pseudo-lidar++ [28] improves the accuracy of depth estimation network using a stereo vision estimation network. SFD [21] uses both the original point cloud and the pseudo point cloud generated by depth estimation network, and fuses them to improve detection accuracy of distant and occluded objects.

2.2.2 Depth Estimation-based Approach

Depth estimation-based methods explicitly predict depth distribution of image features to construct 3D features. These methods are represented by LSS. It predicts both feature distribution in the depth direction and image context information to determine the features of each point of the perspective ray, reducing the loss of image semantics due to depth prediction bias.

BEVDet [7] proposes a multi-view 3D detection framework that includes an image view encoder, view transformer, BEV encoder, and detection head. CaDDN [2] interpolates the sparse depth map into lidar point projection and supervises the depth estimation using depth distribution. MV-FCOS3D++ [15] proposes the pre-training of depth estimation and monocular 3D detection, which significantly enhances the learning ability of 2D backbones.

Our proposed EA-BEV projector explores the refined depth estimation-based approach by using the proposed depth estimation module and edge-aware depth fusion module. EA-BEV framework is enabled to accurately estimate the global depth and the edge regions of objects with sharp depth changes. And “depth jump” problem is effectively al-

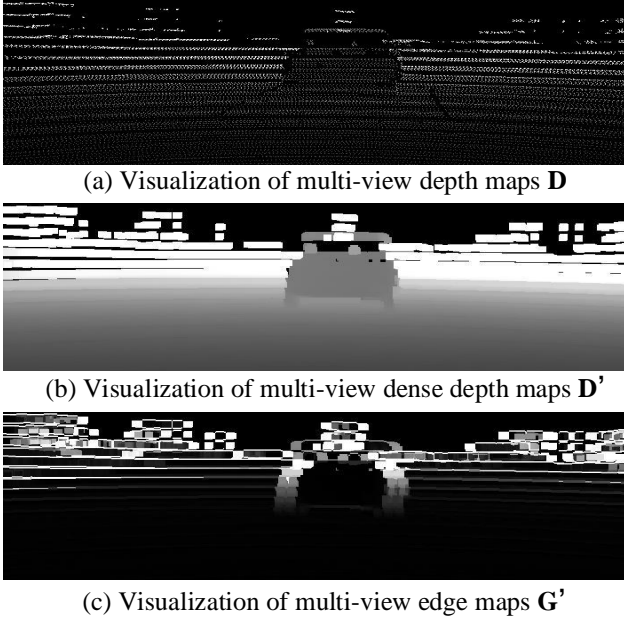


Figure 3. The visualization of (a) multi-view depth maps \mathbf{D} , (b) multi-view dense depth maps \mathbf{D}' , and (c) multi-view edge maps \mathbf{G}' .

leviated, which is meaningful to properly guide subsequent network.

3. Method

In Section 3.1, the overview of LSS framework for Bird’s-Eye-View 3D Object Detection is introduced. In Section 3.2, we introduce our proposed EA-BEV Projector that can be used in any LSS-based method. The proposed edge-aware depth fusion module, semantic DepthNet module and depth estimation module are represented in Section 3.3, Section 3.4, and Section 3.5, respectively. Our proposed sparse depth supervision is included in Section 3.5 and gradient edge depth supervision in 3.6.

3.1. Overview of LSS Framework

In this section, we provide an overview of LSS framework given in Figure 2. LSS framework uses both 2D input (i.e., the 2D multi-view images from camera) and 3D input (i.e., point cloud from lidar) to generate bounding boxes of vehicle, pedestrian, etc.

Given the 2D multi-view camera images, 2D encoder (i.e., swin-Transformer [11]) extracts 2D camera features. These features along with 3D point clouds are fed to our proposed EA-BEV projector to generate the frustum features. After BEV pooling operation, we obtain the camera BEV feature. Lidar features are extracted from 3D point clouds by lidar encoder (i.e., SECOND [27]).

After having both lidar BEV features and camera BEV

features, fusion module and BEV decoder are used to generate the dense BEV features. With detection head, bounding boxes of target objects are generated.

3.2. Edge-aware Bird’s-Eye-View Projector

This section introduces our proposed Edge-aware Bird’s-Eye-View (EA-BEV) projector, which is the orange block shown in Figure 2. EA-BEV projector contains the proposed Edge-aware Depth Fusion module (grey block), Semantic DepthNet Module (yellow block), and Depth Estimation Module (green block).

The inputs of the EA-BEV projector are 2D camera features \mathbf{V}^{cam} and point clouds \mathbf{P} . The point clouds \mathbf{P} are fed to edge-aware depth fusion module to generate the edge-aware depth features \mathbf{F}^{ea} , which are concatenated with 2D camera features \mathbf{V}^{cam} to form 2D-3D concatenated features \mathbf{F}^{concat} . Then predicted depth maps \mathbf{D}^{pred} are generated by depth estimation module.

2D-3D concatenated features \mathbf{F}^{concat} along with 2D camera features \mathbf{V}^{cam} are fed to semantic DepthNet module to generate 2D-3D fused features \mathbf{F}^{fuse} and predicted depth map \mathbf{D}^{DNet} . After the outer multiplication operation, the frustum features are obtained, which is the output of EA-BEV projector.

3.3. Edge-aware Depth Fusion Module

In this section, the proposed edge-aware depth fusion module (grey block in Figure 2) is introduced.

The original point clouds \mathbf{P} are projected to multi-view depth maps, represented as $\mathbf{D} = \{\mathbf{d}_{ij} | i = 1, \dots, N_H; j = 1, \dots, N_W\} \in \mathbb{R}^{N_v * N_H * H_W}$, where N_v represents the number of views, N_H and N_W represent the length and height of depth maps.

Multi-view depth maps \mathbf{D} are divided into blocks in size $k * k$ along x-axis and y-axis, where k is the step size. Then we use the maximum depth value of each block to fill the whole block through expanding operation, which connects most scenes in the point cloud depth map. After blocking and expanding operation, multi-view depth maps \mathbf{D} are transferred to the multi-view dense depth maps \mathbf{D}' with the same dimension.

In the next stage, we calculate gradient of multi-view dense depth map along x-axis and y-axis to extract edge-aware 3D geometry information. Considering each axis has two directions, gradients of dense depth map $\mathbf{G} = \{\mathbf{G}^1, \mathbf{G}^2, \mathbf{G}^3, \mathbf{G}^4\}$, where $\mathbf{G}^k = \{\mathbf{g}_{i,j}^k\}, k = 1, 2, 3, 4$. $\mathbf{g}_{i,j}^1, \mathbf{g}_{i,j}^2, \mathbf{g}_{i,j}^3$, and $\mathbf{g}_{i,j}^4$ are defined as:

$$\begin{cases} \mathbf{g}_{i,j}^1 &= \mathbf{d}'_{i,j} - \mathbf{d}'_{i+k,j}, \\ \mathbf{g}_{i,j}^2 &= \mathbf{d}'_{i,j} - \mathbf{d}'_{i-k,j}, \\ \mathbf{g}_{i,j}^3 &= \mathbf{d}'_{i,j} - \mathbf{d}'_{i,j+k}, \\ \mathbf{g}_{i,j}^4 &= \mathbf{d}'_{i,j} - \mathbf{d}'_{i,j-k}, \end{cases} \quad (1)$$

where $\mathbf{d}'_{i,j}$ is the i^{th} column j^{th} row of multi-view dense depth maps \mathbf{D}' . $\{\mathbf{g}_{i,j}^k\} \in \mathbb{R}^{N_v * N_H * H_W}$ represents one direction of the gradient of multi-view dense depth map.

We take gradients of dense depth map $\mathbf{G} \in \mathbb{R}^{N_v * N_H * H_W * 4}$ as input to the max pooling operation on the last dimension and normalization operation. Multi-view edge maps $\mathbf{G}' \in \mathbb{R}^{N_v * N_H * H_W}$ are obtained to represent the edge of different objects. \mathbf{G}' is scaled to $[0, 1]$ by normalization operation.

As shown in Figure 3 (a), multi-view depth maps \mathbf{D} projected from 3D lidar scanning are sparse, which is not suitable for directly supervising the depth estimation module. Figure 3 (b) shows the multi-view dense depth maps \mathbf{D}' after blocking and expanding operations. Original depth information from depth map is reserved. Main objects in dense depth map are connected, which is beneficial to depth estimation module of the whole scene. In Figure 3 (c), we obtain multi-view edge maps \mathbf{G}' by calculating the maximum gradient value of each pixel along the four directions. The multi-view edge maps \mathbf{G}' represent the maximum depth variation among each block.

After multi-view depth map \mathbf{D} and gradient of multi-view dense depth map \mathbf{G} are obtained, we concatenate \mathbf{D} and \mathbf{G} and feed them to downsampling network to derive the edge-aware 3D features $\mathbf{F}^{ea} \in \mathbb{R}^{N_v * (N_H/8) * (N_W/8) * C_{ea}}$:

$$\mathbf{F}^{ea} = f_{downsample}(\text{Concat}[\mathbf{D} : \mathbf{G}]), \quad (2)$$

where Concat denotes concatenation operation. $f_{downsample}$ is the 8x downsampling network consisting of 3 convolutional layers with stride of 1, 4 and 2 respectively. After the downsampling network, \mathbf{F}^{ea} has the same height and weight as 2D camera features \mathbf{V}^{cam} .

3.4. Semantic DepthNet Module

In this section, we introduce semantic DepthNet module in Figure 4, which is also the yellow block in Figure 2.

As shown in Figure 4, the inputs of semantic DepthNet module are 2D camera features $\mathbf{V}^{cam} \in \mathbb{R}^{N_v * (N_H/8) * (N_W/8) * C_{cam}}$ and 2D-3D concatenate features $\mathbf{F}^{concat} \in \mathbb{R}^{N_v * (N_H/8) * (N_W/8) * C_{concat}}$. Given \mathbf{F}^{concat} , depth distribution estimation $\mathbf{D}^{DNet} \in \mathbb{R}^{N_v * (N_H/8) * (N_W/8) * H_D}$ with its corresponding features $\mathbf{F}^{DNet} \in \mathbb{R}^{N_v * (N_H/8) * (N_W/8) * C_{Dnet}}$ are obtained through the DepthNet (green block in Figure 4).

Given \mathbf{V}^{cam} , context features $\mathbf{F}^{context}$ are obtained through 2 convolutional layers and skip connection. Then fused features \mathbf{F}^{fused} are obtained through concatenation operation $\mathbf{F}^{fused} = \text{Concat}[\mathbf{F}^{context} : \mathbf{F}^{DNet}]$. Predicted depth map \mathbf{D}^{DNet} and fused features \mathbf{F}^{fused} are the output of semantic DepthNet module.

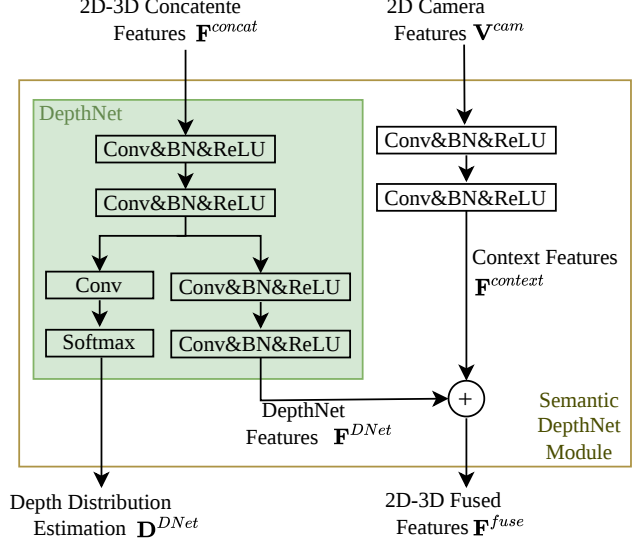


Figure 4. Overview of semantic DepthNet module. Given 2D camera features \mathbf{V}^{cam} and 2D-3D concatenate features \mathbf{F}^{concat} , predicted depth map \mathbf{D}^{DNet} and 2D-3D fused features \mathbf{F}^{fused} are generated by semantic DepthNet module.

3.5. Depth Estimation Module

This section introduces our proposed depth estimation module, sparse depth supervision and gradient edge depth supervision.

2D-3D concatenate features \mathbf{F}^{concat} are fed to depth estimation module (green block in Figure 2) to generate predicted depth map $\mathbf{D}^{pred} \in \mathbb{R}^{N_v * N_H * N_W * H_D}$. Depth estimation module is consisted of three deconvolution layers with stride of two, and has the effect of 8x upsampling.

To supervise the predicted depth map \mathbf{D}^{pred} , multi-view depth maps \mathbf{D} are used as the ground-truth. Since multi-view depth maps \mathbf{D} are sparse, we propose sparse depth supervision, where only non-zero pixels in the ground-truth depth map are used to calculate the loss. Thus disturbance from zero-valued pixels is effectively eliminated. To focus on the foreground objects (more objects appear in background), focal loss is embedded in sparse depth loss L_{SD} for sparse depth supervision. Sparse depth loss L_{SD} is defined as:

$$L_{SD} = \sum_{i=1}^n \sum_{c=1}^{H_D} -\alpha_c (1 - y_{i,c})^\gamma \log(\hat{y}_{i,c}), \quad (3)$$

where n is the number of non-zero pixels in ground-truth \mathbf{D} . H_D denotes the classes of predicted depth. Here ground-truth \mathbf{D} is transferred to one-hot vectors. $\hat{y}_{i,c}$ is the value of c^{th} class of i^{th} one-hot vector of non-zeros pixels in \mathbf{D} , while $y_{i,c}$ is from the corresponding pixels in predicted depth map \mathbf{D}^{pred} . α_c denotes the weight and γ denotes the predefined hyper-parameter for focal loss.

Method	Modality	Resolution	mAP	NDS	Latency(ms)
BEVFormer [32]	C	900×1600	41.6	51.7	-
CenterPoint [30]	L	-	59.6	66.8	80.7
TransFusion-L [22]	L	-	65.5	70.2	-
FUTR3D [3]	C+L	-	64.5	68.3	321.4
MVP [17]*	C+L	-	66.1	70.0	187.1
PointAugmenting † [19]	C+L	-	66.8	71.0	-
TransFusion [22]	C+L	448×800	67.5	71.3	156.6
DeepInteraction [29]	C+L	640×1600	69.9	72.6	204.1
BEVDepth-R50 [25]	C	256×704	35.1	47.5	110.3
+EA-BEV	C	256×704	40.4	48.2	114.8
BEVFusion [31]	C+L	256×704	68.5	71.4	119.2
+EA-BEV	C+L	256×704	69.4	71.8	123.6
BEVFusion [10]	C+L	448×800	69.6	72.1	190.3
+EA-BEV	C+L	448×800	70.1	72.6	194.9

Table 1. Comparison results of 3D object detection on nuScenes validation dataset. † means using TTA(test-time augmentation), * is reported from [31]. After using our proposed EA-BEV projector, mAP scores of LLS-based baseline methods BEVDepth-R50 [25], BEVFusion [31] and BEVFusion [10] increase 5.3%, 0.9% and 0.5%, respectively. While the increment of inference time is only less than 5%.

3.6. Gradient Edge Depth Supervision

Sparse depth supervision makes accurately use of information of depth maps. But depth maps are sparse, affecting accuracy and convergence speed of depth estimation module. Therefore, we propose gradient edge depth supervision to focus on the edge of each object, by using multi-view dense depth maps \mathbf{D}' as ground truth and multi-view edge maps \mathbf{G}' as weight to alleviate the “depth jump” problem. Gradient edge depth loss L_{GED} for supervision is defined:

$$L_{GED} = \sum_{i=1}^m \sum_{c=1}^{H_D} -\alpha_c (1 - p_{i,c})^\gamma \log(\hat{p}_{i,c}) * w_i, \quad (4)$$

where m is the number of pixels in predicted depth map \mathbf{D}^{pred} . H_D denotes the classes of predicted depth. $p_{i,c}$ denotes the value of c^{th} class of the i^{th} pixel from predicted depth map \mathbf{D}^{pred} , $\hat{p}_{i,c}$ is the corresponding pixel in ground-truth depth map \mathbf{D}' , and w_i is the corresponding pixel value of \mathbf{G}' . α_c denotes the weight and γ denotes the predefined hyper-parameter for focal loss.

The total loss L_{total} is defined as:

$$L_{total} = L_{SD} + L_{GED} + L_{cls} + L_{box}, \quad (5)$$

where L_{SD} and L_{GED} represent sparse depth loss and gradient edge depth loss defined in Eqn (3) and Eqn (4), respectively. L_{cls} and L_{box} are classification loss and bounding box loss in the detection head.

4. Experiments

4.1. Implementation Details

In our experiments, we use BEVFusion [31]/ BEVFusion [10]/ BEVDepth [25] as the baseline to verify the effectiveness and efficiency of our proposed EA-BEV.

When using BEVFusion as baseline, we follow the same parameter settings as in [31]. Epoch is set to 6, batch size is set to 4, learning rate is set to 0.0002 and Cosine Annealing strategy is used. When using BEVFusion [10], learning rate is set to 0.0001, weight Decay is set to 0.05, batch size is set to 2. When using BEVDepth [25], learning rate is set to 0.0002, batch size is set to 2, weight Decay is set to 1e-7.

In the blocking and expanding operation of edge-aware depth reconstruction module, step size k is set to 7. The number of views N_v is set to 6. Height and weight of depth maps N_H and N_W are set to 256 and 704. The number of channels C_{ea} , C_{cam} , C_{dnet} and $C_{context}$ are set to 64,256,128 and 128, respectively. The classes of predicted depth H_D is set to 118. Both L_{SD} and L_{GED} adopt focal Loss, and γ and α_c are set to 2.0 and 0.25, respectively. Our training environment is on a server with 8*NVIDIA A100 GPU and AMD EPYC 7402 CPU.

4.2. Comparison Results

4.2.1 nuScenes 3D Object Detection

In order to evaluate the effectiveness of our proposed EA-BEV Projector, we conduct comparison experiments on nuScenes Dataset. This dataset contains 40k labeled samples, with 23 different classes. We use mean Average Precision (mAP) and nuScenes detection score (NDS) as evalu-

Method	Modality	mAP \uparrow	NDS \uparrow	mATE \downarrow	mASE \downarrow	mAOE \downarrow	mAVE \downarrow	mAAE \downarrow
BEVDet [7]	C	42.2 \dagger	48.2 \dagger	0.529	0.236	0.396	0.979	0.152
BEVFormer [32]	C	44.5	53.5	0.582	0.256	0.375	0.378	0.126
BEVDet4D [6]	C	45.1 \dagger	56.9 \dagger	0.511	0.241	0.386	0.301	0.121
Pointpillars [5]	L	30.5	45.3	0.517	0.290	0.500	0.316	0.368
SECOND [27]	L	52.8	63.3	-	-	-	-	-
CenterPoint [16]	L	60.3	67.3	0.262	0.239	0.361	0.288	0.136
PointAugmenting [19]	C+L	66.8 \dagger	71.0 \dagger	0.253	0.235	0.354	0.266	0.123
MVP [17]	C+L	66.4	70.5	0.263	0.238	0.321	0.313	0.134
TransFusion [22]	C+L	68.9	71.6	0.259	0.243	0.359	0.288	0.127
CMT [9]	C+L	70.4	73.0	0.299	0.241	0.323	0.240	0.112
DeepInteraction-base [29]	C+L	70.8	73.4	0.257	0.240	0.325	0.245	0.128
BEVFusion [10]	C+L	71.3	73.3	0.250	0.240	0.359	0.254	0.132
+EA-BEV	C+L	71.5	73.5	0.252	0.238	0.336	0.270	0.132

Table 2. Comparison results of 3D object detection on nuScenes test dataset. \dagger means using TTA.

Method	Modality	Drivable	Ped.Cross.	Walkway	Stop Line	Carpark	Divider	Mean
OFT [13]	C	74.0	35.3	45.9	27.5	35.9	33.9	42.1
LSS [8]	C	75.4	38.8	46.3	30.3	39.1	36.5	44.4
CVT [33]	C	74.3	36.8	39.9	25.8	35.0	29.4	40.2
PointPillars [5]	L	72.0	43.1	53.1	29.7	27.7	37.5	43.8
CenterPoint [16]	L	75.6	48.4	57.5	36.5	31.7	41.9	48.6
PointPainting [18]	C+L	75.9	48.5	57.1	36.9	34.5	41.9	49.1
MVP [17]	C+L	76.1	48.7	57.0	36.9	33.0	42.2	49.0
BEVFusion [31]	C+L	85.5	60.5	67.6	52.0	57.0	53.7	62.7
+EA-BEV	C+L	85.8	61.1	68.0	52.3	56.8	54.5	63.1

Table 3. Comparison results of BEV map segmentation task on nuScenes validation Dataset. We report the IoU score of drivable area, pedestrian cross, walkway, stop line, carpark, divider and the mean IoU score. The mean IoU score increases 0.4 % after adding our proposed EA-BEV projector to the baseline method BEVFusion [31].

ation indicators. Mean mAP score and mean NDS score of 10 foreground classes on validation set are reported.

Table 1 reports experiment results of nuScenes 3D object detection validation dataset. Our proposed EA-BEV projector can be added to any LSS-based baseline methods [25, 31, 10] with negligible increment of inference time. When using BEVDepth-R50 [25] as baseline, mAP score and NDS score increase 5.3% and 0.7% after applying the proposed EA-BEV projector. On BEVFusion [31] baseline, mAP score and NDS score increase 0.9% and 0.4%. On BEVFusion [10] baseline, mAP score and NDS score increase 0.5% and 0.5%.

In Table 2, we report the experiment results of nuScenes 3D object detection test dataset. On BEVFusion [10] baseline, mAP score and NDS score increase 0.2% and 0.2%.

4.2.2 nuScenes BEV Map Segmentation

To evaluate generalization capability, experiments on nuScenes BEV Map Segmentation (i.e., semantic segmentation) task are conducted. Following the same training

strategy of baseline method BEVFusion [31], we report the Intersection-over-Union (IoU) score of drivable area, pedestrian cross, walkway, stop line, carpark, divider. A single model that jointly performs binary segmentation for all classes, instead of following conventional approach, is employed to train a separate model for each class

In Table 3, we report comparison results of BEV map segmentation task on nuScenes validation Dataset. After adding the proposed EA-BEV projector to baseline method BEVFusion [31], the mean IoU score increase 0.4 %, which demonstrates generalization capability.

4.3. Ablation Study

To examine effectiveness of each component, we provide ablation study in Table 4. We use BEVFusion [31] as baseline method. C means adding context features $F^{context}$ in semantic DepthNet module; DEN represents the depth estimation module; SDL represents the sparse depth loss; CONCAT-G represents concatenating the gradient of multi-view dense depth map \mathbf{G} in edge-aware depth fusion module; EGDL represents the edge gradient depth loss. In-

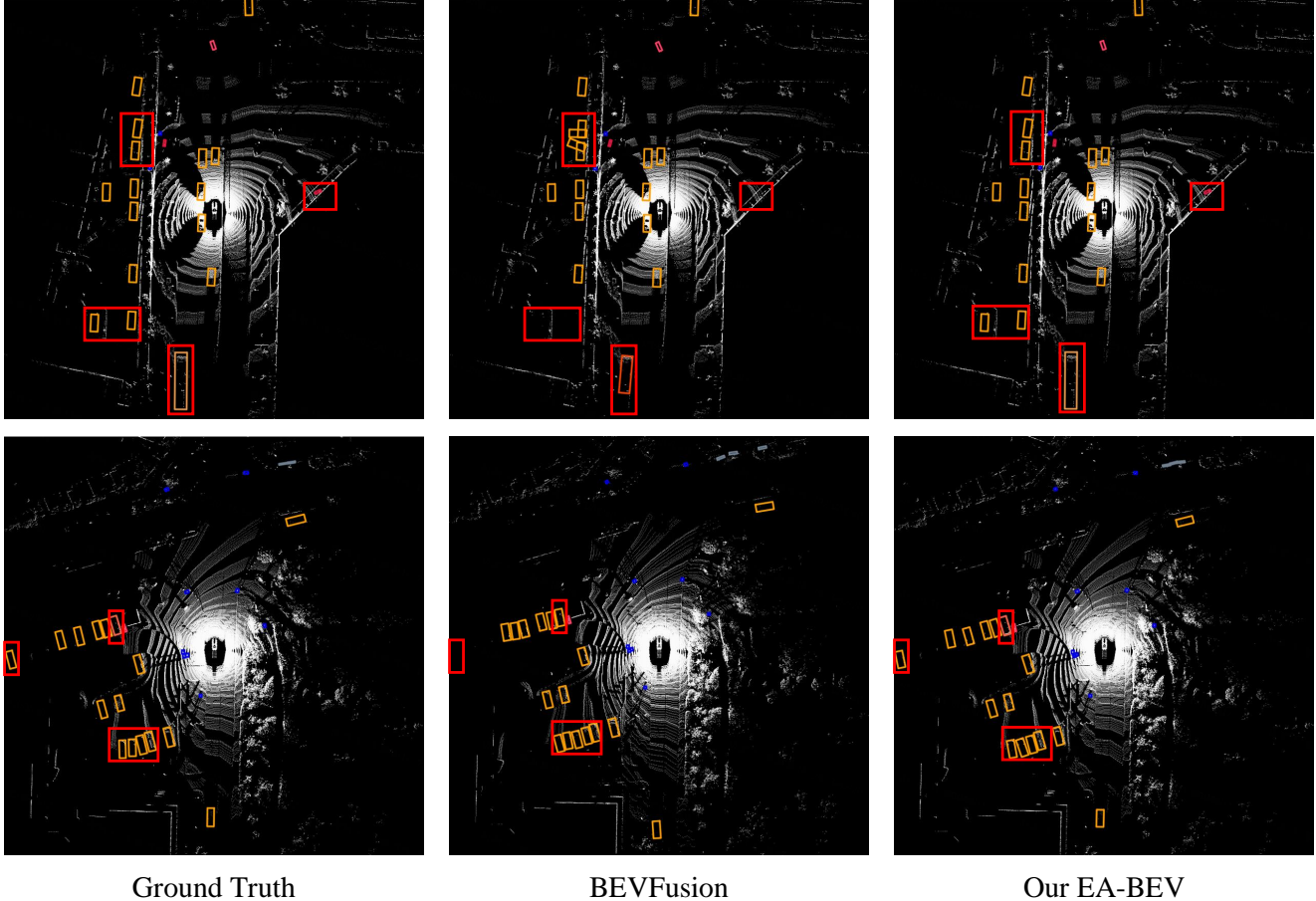


Figure 5. Visualization of the nuScenes 3D object detection validation dataset. From the left to the right, we provide results of ground-truth, baseline method BEVFusion [31] before and after adding our proposed EA-BEV projector. We can observe that results after adding our proposed EA-BEV projector are better than before.

C	DEN	SDL	CONCAT-G	EGDL	mAP	NDS
×	×	×	×	×	68.5	71.4
✓	×	×	×	×	68.6	71.5
✓	✓	✓	×	×	68.7	71.6
✓	✓	✓	✓	×	69.1	71.7
✓	✓	✓	✓	✓	69.4	71.8

Table 4. Ablation study of 3D object detection on nuScene validation dataset. C: context feature $F^{context}$ in semantic DepthNet module, DEN: depth estimation module, SDL: sparse depth loss, CONCAT-G: concatenate gradient of multi-view dense depth map G in edge-aware depth fusion module, EGDL: edge gradient depth loss.

creased mAP scores and NDS scores in Table 4 demonstrate the effectiveness of mentioned components.

Table 5 provides performances on nuScenes 3D object detection validation dataset when using different step size k of blocking and expanding operation in edge-aware

k	mAP	NDS
3	68.9	71.6
5	69.1	71.6
7	69.4	71.8
9	68.4	71.4

Table 5. Performances on nuScenes 3D object detection validation dataset when using different step k of blocking and expanding operation in edge-aware depth fusion module.

depth fusion module. We use BEVFusion [31] as baseline method. The best mAP score and NDS score are achieved when $k = 7$.

4.4. Qualitative Evaluation

We provide visualization results (Figure 5 and Figure 6) to demonstrate the effectiveness of our proposed EA-BEV projector on nuScenes BEV map Segmentation and nuScenes 3D object detection. We show the visual-

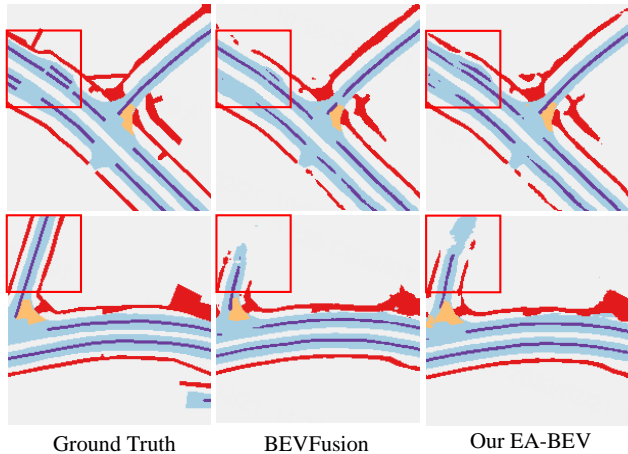


Figure 6. Visualization of the nuScenes BEV map segmentation validation dataset. From the left to the right, we provide results of ground-truth, baseline method BEVFusion [31] before and after adding EA-BEV projector.

ization results of nuScenes 3D object detection validation dataset In Figure 5. We provide the experiment results of ground-truth, baseline method BEVFusion [31] and baseline method adding our proposed EA-BEV projector in the first column, second column and third column. The cars are shown in yellow, the pedestrian shown in blue and truck shown in pink. We can capture more target objects by adding our proposed EA-BEV projector than using the baseline method BEVFusion [31] only.

In Figure 6, we provide the qualitative evaluation on nuScenes BEV map segmentation validation dataset. From the left to the right, we provide the results of ground-truth, baseline method BEVFusion [31] and baseline method adding our proposed EA-BEV projector. The drivable area are shown in blue, the lane divider shown in purple, the walkway shown in red, the crosswalk shown in pink. From the red bounding boxes, we can observe that the results of adding our proposed EA-BEV projector is better than using the baseline method only.

5. Conclusion

This paper proposes EA-BEV projector to alleviate the “depth jump” problem and better utilize depth information to supervise depth prediction tasks on 3D outdoor object detection. Our proposed EA-BEV projector is plug-and-play and can be used in any LSS-based methods. Moreover, we propose edge-aware depth fusion module and gradient edge depth supervision, and depth estimation module to generate estimated depth distribution more accurately. To validate effectiveness and efficiency, we conduct experiments on nuScenes 3D object detection benchmarks and BEV map segmentation benchmarks. It is expected that our proposed EA-BEV projector can inspire further re-

searches on depth estimation of 3D outdoor object detection.

References

- [1] Lu C., Molengraft van de M. J. G., and Dubbelman G. Monocular semantic occupancy grid mapping with convolutional variational encoder–decoder networks. *IEEE Robotics and Automation Letters*, pages 445–452, 2019. 2
- [2] Reading C., Harakeh A., Chae J., and Waslander S. L. Categorical depth distribution network for monocular 3d object detection. In *in Proceedings of the IEEE/CVF Conference on Computer Vision and Pattern Recognition*, pages 8555–8564, 2021. 2, 3
- [3] Xuanyao Chen, Tianyuan Zhang, Yue Wang, Yilun Wang, and Hang Zhao. Futr3d: A unified sensor fusion framework for 3d detection. *arXiv preprint arXiv:2203.10642*, 2022. 6
- [4] Caesar H., Bankiti V., Lang A. H., Vora S., Liong V. E., Xu Q., Krishnan A., Pan Y., Baldan G., and Beijbom O. nuscenes: A multimodal dataset for autonomous driving. In *CVPR*, 2020. 2
- [5] Lang A. H., Vora S., Caesar H., Zhou L., Yang J., and Beijbom O. Pointpillars: Fast encoders for object detection from point clouds. In *in IEEE Conference on Computer Vision and Pattern Recognition*, 2019. 7
- [6] Huang J. and Huang G. Bevdet4d: Exploit temporal cues in multi-camera 3d object detection. *arXiv preprint arXiv:2203.17054*, 2022. 7
- [7] Huang J., Huang G., Zhu Z., and Du D. Bevdet: High-performance multi-camera 3d object detection in bird-eye-view. *arXiv preprint arXiv:2112.11790*, 2021. 1, 2, 3, 7
- [8] Philion J. and Fidler S. Lift, splat, shoot: Encoding images from arbitrary camera rigs by implicitly unprojecting to 3d. In *in European Conference on Computer Vision*, pages 194–210, 2020. 1, 3, 7
- [9] Yan Junjie, Liu Yingfei, Sun Jianjian, Jia Fan, Li Shuailin, Wang Tiancai, and Zhang Xiangyu. Cross modal transformer via coordinates encoding for 3d object detection. *arXiv preprint arXiv:2301.01283*, 2023. 7
- [10] Tingting Liang, Hongwei Xie, Kaicheng Yu, Zhongyu Xia, Zhiwei Lin, Yongtao Wang, Tao Tang, Bing Wang, and Zhi Tang. Bevfusion: A simple and robust lidar-camera fusion framework. In *Neural Information Processing Systems (NeurIPS)*, 2022. 2, 6, 7
- [11] Ze Liu, Yutong Lin, Yue Cao, Han Hu, Yixuan Wei, Zheng Zhang, Stephen Lin, and Baining Guo. Swin transformer: Hierarchical vision transformer using shifted windows. In *Proceedings of the IEEE/CVF international conference on computer vision*, pages 10012–10022, 2021. 4
- [12] Li Q., Wang Y., Wang Y., and Zhao H. Hdmapnet: An online hd map construction and evaluation framework. *arXiv preprint arXiv:2107.06307*, 2021. 2
- [13] Thomas Roddick, Alex Kendall, and Roberto Cipolla. Orthographic feature transform for monocular 3d object detection. In *In BMVC*, 2019. 7
- [14] Chen S., Wang X., Cheng T., Zhang Q., Huang C., and Liu W. Polar parametrization for vision-based surround-view 3d detection. *arXiv preprint arXiv:2206.10965*, 2022. 3

- [15] Wang T., Lian Q., Zhu C., Zhu X., and Zhang W. Mv-fcos3d++: Multi-view camera-only 4d object detection with pretrained monocular backbones. *arXiv preprint arXiv:2207.12716*, 2022. 2, 3
- [16] Yin T., Zhou X., and Krähenbühl Philipp. Center-based 3d object detection and tracking. In *CVPR*, 2021. 7
- [17] Yin T., Zhou X., and Krähenbühl Philipp. Multimodal virtual point3d detection. *M. Ranzato, A. Beygelzimer, Y. N. Dauphin, P. Liang and J.W. Vaughan, Eds.*, pages 16494–16507, 2021. 6, 7
- [18] Sourabh Vora, Alex H Lang, Bassam Helou, and Oscar Beijbom. Pointpainting: sequential fusion for 3d object detection. In *In CVPR*, 2020. 7
- [19] Chunwei Wang, Chao Ma, Ming Zhu, and Xiaokang Yang. Pointaugmenting: Cross-modal augmentation for 3d object detection. In *Proceedings of the IEEE/CVF Conference on Computer Vision and Pattern Recognition*, pages 11794–11803, 2021. 6, 7
- [20] T. Wang, X. Zhu, J. Pang, and D. Lin. Fcos3d: Fully convolutional one-stage monocular 3d object detection. *arXiv preprint arXiv:2104.10956*, 2021. 2
- [21] Xiaopei Wu, Liang Peng, Honghui Yang, Liang Xie, Chenxi Huang, Chengqi Deng, Haifeng Liu, and Deng Cai. Sparse fuse dense: Towards high quality 3d detection with depth completion. *arXiv preprint arXiv:2203.09780*, 2022. 2, 3
- [22] Bai X., Hu Z., Zhu X., Huang Q., Chen Y., Fu H., and Tai C. Transfusion: Robust lidar-camera fusion for 3d object detection with transformers. In *CoRR*, 2022. 6, 7
- [23] Zhou Xingyi, Wang Dequan, and Krähenbühl Philipp. Objects as points. *arXiv preprint arXiv:1904.07850*, 2019. 2
- [24] Liu Y., Yan J., Jia F., Li S., Gao Q., Wang T., Zhang X., and Sun J. Petrv2: A unified framework for 3d perception from multi-camera images. *arXiv preprint arXiv:2206.01256*, 2022. 2, 3
- [25] Li Y., Ge Z., Yu G., Yang J., Wang Z., Shi Y., Sun J., and Li Z. Bevdepth: Acquisition of reliable depth for multi-view 3d object detection. *arXiv preprint arXiv:2206.10092*, 2022. 1, 2, 6, 7
- [26] Wang Y., Guizilini V. C., Zhang T., Wang Y., Zhao H., and Solomon J. Detr3d: 3d object detection from multi-view images via 3d-to-2d queries,” in conference on robot learning. In *PMLR*, pages 180–191, 2022. 2
- [27] Yan Y., Mao Y., and Li B. Second: Sparsely embedded convolutional detection. In *Sensors*, 2018. 4, 7
- [28] You Y., Wang Y., Chao W.-L., Garg D., Pleiss G., Hariharan B., Campbell M., and Weinberger K. Q. Pseudo-lidar++: Accurate depth for 3d object detection in autonomous driving. In *in ICLR*, 2020. 2, 3
- [29] Zeyu Yang, Jiaqi Chen, Zhenwei Miao, Wei Li, Xiatian Zhu, and Li Zhang. Deepinteraction: 3d object detection via modality interaction. In *NeurIPS*, 2022. 6, 7
- [30] Tianwei Yin, Zhou Xingyi, and Philipp Krahenbuhl. Centerbased 3d object detection and tracking. In *Proceedings of the IEEE/CVF Conference on Computer Vision and Pattern Recognition*, pages 11784–11793, 2021. 6
- [31] Liu Z., Tang H., Amini A., Yang X., Mao H., Rus D., and Han S. Bevfusion: Multi-task multi-sensor fusion with unified bird’s-eye view representation. In *CoRR*, 2022. 1, 2, 6, 7, 8, 9
- [32] Li Z., Wang W., Li H., Xie E., Sima C., Lu T., Qiao Y., and Dai J. Bevformer: Learning bird’s-eye-view representation from multicamera images via spatiotemporal transformers. *arXiv preprint arXiv:2203.17270*, 2022. 2, 6, 7
- [33] Bardy Zhou and Philipp Krähenbühl. Cross-view tranformer for real-time map-view semantic segmentation. In *In CVPR*, 2022. 7